

ARTICLE TEMPLATE

A Spatial-statistical model to analyse historical rutting data

N. O. A. S Jourdain^a, I. Steinsland^a, M. Birkhez-Shami^a, D. Gryteselv^b, D. Siebert^b
and A. Klein-Paste^a

^aNorwegian University of Science and Technology (NTNU), Trondheim, Norway;

^bStatens Vegvesen, Trondheim, Norway

ARTICLE HISTORY

Compiled January 9, 2024

ABSTRACT

Pavement rutting poses a significant challenge in flexible pavements, necessitating costly asphalt resurfacing. To address this issue comprehensively, we propose an advanced Bayesian hierarchical framework of latent Gaussian models with spatial components. Our model provides a thorough diagnostic analysis, pinpointing areas exhibiting unexpectedly high rutting rates. Incorporating spatial and random components, and important explanatory variables like annual average daily traffic (traffic intensity), pavement type, rut depth and lane width, our proposed models account for and estimate the influence of these variables on rutting. This approach not only quantifies uncertainties and discerns locations at the highest risk of requiring maintenance, but also uncover spatial dependencies in rutting (millimetre/year). We apply our models to a data set spanning eleven years (2010-2020). Our findings emphasize the systematic unexpected spatial rutting effect, where more of the rutting variability is explained by including spatial components. Pavement type, in conjunction with traffic intensity, is also found to be the primary driver of rutting. Furthermore, the spatial dependencies uncovered reveal road sections experiencing more than 1 millimeter of rutting beyond annual expectations. This leads to a halving of the expected pavement lifespan in these areas. Our study offers valuable insights, presenting maps indicating expected rutting, and identifying locations with accelerated rutting rates, resulting in a reduction in pavement life expectancy of at least 10 years.

KEYWORDS

Flexible pavement; predictive maintenance; rutting; spatial-statistical model; uncertainty

1. Introduction

Pavement maintenance is essential to ensure road safety and prevent excessive depreciation of roads. Rutting is a major problem in flexible pavement structures and it is one of the major causes why pavements need asphalt resurfacing. Rutting is a distress mechanism that causes longitudinal surface depressions within the wheel path of the asphalt concrete layer. It can substantially affect traffic safety (Hao *et al.* 2009) due to impaired steerability and friction reduction due to standing water in the ruts. Ruts occur under the combined actions of traffic loads (Zhang *et al.* 2017) and is affected by environmental conditions, e.g., climate, seepage, temperature, weather (Ranadive and

Tapase 2016, Gudipudi *et al.* 2017, Zhang *et al.* 2023), and the inherent viscoelastic properties of the construction (e.g., thickness in surface layers or voids in the mixture Gu *et al.* 2017, Cheng *et al.* 2023). Rutting may occur at the various layers (Lea and Harvey 2015, Alhasan *et al.* 2018) or various stages (e.g., primary, secondary or tertiary) (Korkiala-Tanttu and Dawson 2007, Al-Khateeb and Basheer 2009, Gupta *et al.* 2014) of a constructed pavement. In cold climates, rutting often determines the longevity of the top layer of flexible pavements (Lundy *et al.* 1992), and the dominating mechanism is wear from studded tires (Snilsberg 2008), as opposed to permanent deformations in the mastic.

The rut depth can be effectively measured by laser profilometry (Thodesen *et al.* 2012). Many road agencies or road maintenance contractors map their road network regularly as input for their Pavement Management System (PMS). In Norway, all state roads are scanned every year, and this measurement program have been providing pavement condition data into a single database (ROSITA) since 2010. The Norwegian PMS system can provide automatically generated reports, for example which sections exceed the maximum allowed rut depth defined in the maintenance standards. However, deeper diagnostic analysis to identify areas that exhibit unexpectedly high rutting rates still requires manual labor. Such type of data analysis is typically only initiated based on suspicion and are very time consuming.

Acknowledging that the value of long time series of pavement condition data has not been fully utilized, the Norwegian Public Roads Administration initiated a research project that aims for more automated pavement diagnostics. Our working hypothesis is that advanced statistical analysis of the available data can provide a better understanding of how the pavement condition of a whole network develops and allow automated identification of segments that perform better or worse than expected. Moving from “manual, suspicion-based” diagnostics towards automated identification of problem areas enables pavement managers to concentrate their diagnostic resources on finding the correct countermeasures, rather than finding the problem areas. Identifying sections with unexpectedly high rutting levels requires that one compares with the ‘expected performance’ in terms of rutting.

Several empirical models have been proposed in the past to predict the performance of pavements (Hu *et al.* 2022, Yao *et al.* 2023, Yu *et al.* 2023) and these models typically include rutting. Empirical models usually relate the accumulation of distresses (e.g., rut, roughness, cracks) in the pavement layers to the load repetitions (annual average daily traffic) and other affecting factors (e.g., pavement or asphalt type, weather, width of the road, layer thickness). Empirical models are known to suffer from limited applicability (Gupta *et al.* 2014), so when the conditions (for example road construction, weather conditions or damage mechanisms) during the data collection differs from the conditions where the model is applied, one cannot expect to get reasonable results. Empirical models developed for pavement wear in cold climates exists (Jacobson and Wågberg 2005), but the challenge of limited predictability remains present. Calculating the expected rutting for sections based on an empirical model is therefore likely to rather large uncertainty.

Another modelling framework for predicting pavement performance from local historical data has been based on foundation layers and stages of deterioration and models of transition probability matrices (TPMs) (Chou *et al.* 2008, Pérez-Acebo *et al.* 2019, Yamany and Abraham 2020). This has some weaknesses, including its usability for the prediction of conditions based on a limited number of discrete classes (Vermunt *et al.* 1999, Pulugurta *et al.* 2009, Standfield *et al.* 2014) increasing imprecision and inaccuracy when assigning TPMs to the various deterioration stages; limitation in their

generalizability to other flexible pavement data; and their lack of potential to account for spatial heterogeneity in the data (Saba *et al.* 2006, Chen and Mastin 2016)

Spatial models can provide additional explanation by accounting for trends in location. In the case of pavements, it is likely that sections close to each other behave more similar than sections that are far apart. These location components cannot explain the cause of the behaviour but they do have explanatory value and can be utilized to identify ‘hotspots’, predict future rut depths and quantify uncertainties.

Spatial models have been proposed for understanding pavement behaviour earlier (Lea and Harvey 2015, Alhasan *et al.* 2018, Ebrahimi *et al.* 2019). Lea and Harvey (2015) considered the applicability of spatial variability models on a test pavement containing a modified binder constructed for heavy vehicle simulator testing and found that the implementation of the spatial statistical techniques gave good insights concerning pavement variability following the complexity of pavement construction. (Alhasan *et al.* 2018), on the other hand, extended the more traditional mechanistic-empirical pavement prediction modelling framework by incorporating spatial variability and uncertainty in pavement foundation layers. (Ebrahimi *et al.* 2019) estimated asphalt surfacing lifetime for open road infrastructure on Norway road network (excluding bridges and tunnels) in Troms, Sør-Trøndelag and Vest-Agder. Their analysis showed that narrower road width was noted to result in shorter pavement lifetimes, particularly in Troms, where studded tires are used one month earlier than other locations, e.g., Vestland or Trøndelag in Norway.

Our primary goal is to develop spatial-statistical models that can pinpoint pavement locations exhibiting unexpected and pronounced spatial rutting effects. To achieve this, we employ a hierarchical Bayesian framework comprising latent Gaussian models (LGMs) that encompass both random and spatial components. Latent Gaussian models have been used in various statistical analyses, as demonstrated by their applications in a multitude of fields (e.g., Dey *et al.* 2000, Chu *et al.* 2005, Banerjee *et al.* 2008, Rue *et al.* 2009b). These models offer a high degree of flexibility and explicitly account for model dependence. They can approximate entire processes defined over continuous domains and provide probabilistic predictions (Lindgren and Rue 2015). In our specific case, the rutting phenomenon on road surfaces persists regardless of whether it is directly observed, with the latent fields serving as the authentic representation of this rutting. A crucial premise underlying spatial models is that observations situated in close proximity to one another in the spatial domain exhibit greater similarity than those positioned further apart. For a broad class of LGMs, the Integrated Nested Laplace Approximation approach (INLA, Rue *et al.* 2009a) proves to be an apt tool for performing Bayesian inference.

The proposed models are based on historical rutting observations and a selection of explanatory variables known to influence pavement rutting. These variables include pavement type, Average Annual Daily Traffic (AADT), rut depth from the previous year and lane width. The inclusion of these variables is grounded in existing knowledge of factors that significantly influence rutting in road surfaces (Chan *et al.* 2010, Lang 2012, Thodesen *et al.* 2012, Ebrahimi *et al.* 2019, Yan *et al.* 2020, Zhao *et al.* 2020, Pan *et al.* 2021, Li *et al.* 2023). Rutting is a complex phenomenon, and the depth of rutting observed in the previous year is a key factor in predicting future rutting. Deeper rut depths from the previous year are expected to correlate with increased rutting in the current year, and this relationship is incorporated into the model. Additionally, lane width is considered as a contributing factor to rutting rates. It is logical to assume that narrower roads are more prone to higher rutting rates due to the limited space for motorists to maneuver. However, it’s important to note that the effect of lane width

on rutting is contingent on the intensity of traffic. A critical element in our model is the role of Average Annual Daily Traffic (AADT) on the pavement. Rutting, as we argue, is contingent on the presence of AADT or the load imposed by traffic. Without traffic loading, certain forms of pavement deterioration, such as cracks and roughness, may occur, but rutting is improbable. This hypothesis aligns with prior research on the prediction of pavement variability and deterioration, as illustrated in the work of Hao et al. (2009) and Vedvik (2021) (Hao *et al.* 2009, Vedvik 2021). In this context, we emphasize a linear approximation for data processing, with the constraint that it passes through the origin. Furthermore, our model is designed with a standardized data approach, where the intercept is set to zero by design, ensuring consistency in the methodology.

As proof of concept, our proposed models are applied to eleven years (2010-2020) of pavement rutting data for one road stretch; the European highway route E14, stretching 67.1 kilometres from Stjørdal, Norway to Storlien on the Swedish border. We identify areas with unexplained or accelerated rutting and determine which explanatory variables are most important to rutting development. A detailed description of the data used and data cleaning process is given in Section 2. Model notation, formulation and evaluation criteria are given in Section 3. Results and discussion are given in 4. Section 5 explains how road authorities can use the model, based on the results.

2. Materials

2.1. Data source

The data material used in this research is obtained from the Norwegian Road Database (NVDB) and the *Rosita* database. The NVDB is primarily developed by the Norwegian Public Roads Administration (NPRA), the road authority for national roads, including managing, researching, planning, building, and operating. In 2022, NVDB consisted of 93 500 kilometres of public roads, including national roads (state-owned, 10,500 kilometres), county roads (44 000 kilometres) and municipal roads (39 000 kilometres) (Stephansen 2022). The *Rosita* database, which stores extensive and calculated data from measuring systems (see Section 2.3), was made available for use in this study.

2.2. Area of study

The area of our case study is the highway road in the county of Trøndelag in Norway; the European route E14 — Stjørdal, Norway to Storlien on the Norwegian-Swedish border. The road is considered as a major highway consisting of flexible bituminous mixtures, and is located at latitude $63^{\circ} 19' 1.80''$ N and longitude $14^{\circ} 11' 24.00''$ E. It is constructed and maintained by the Norwegian Public Roads Administration, where routine and periodical maintenance systems are applicable. The road is 67.1 kilometres long, and most of it consists of two lanes divided with safeguards. From Stjørdal and up to (\sim) 2.5 kilometres, it is four lanes; two lanes in each driving direction. Road stretches with ordinary two-lanes are approximately 6 metres wide, and up to 13 metres wide where there are four lanes. According to the Norwegian Public Roads Administration, the expected lifetime of the road is 20 – 30 years after construction. The normal annual rut depths of the road ranged from 0 – 41 millimetres, and are measured at 20-metre sections along the road. The climate along European highway

route E14 is influenced by its northern location and can be classified as a subarctic or cold-temperate climate. The specific climate zone along this route can vary depending on the time of year and the exact location with maximum temperatures, on average, ranging from -2°C to 2°C in the winter; 5°C to 12°C in the spring; 15°C to 22°C in the summer; and 10°C to 15°C in the autumn (Sygna and O'Brien 2001, Institutt 2010). For analysis purposes, one lane in the driving direction of Stjørdal to Storlien on the Swedish border (lane 1) is used. Also, the measured rut depth values at 20-metre sections (hereafter refer to as road segments) are used. Following Vedvik (2021) all variables that explain the expected annual rut depth are related to the 20-metre road segments at geographical locations taken in the year 2020. There are 3355 road segments measured for annual rut depth.

2.3. Data

The available explanatory variables for expected rut depth includes, traffic load in terms of annual average daily traffic (AADT), pavement or asphalt type (three categories), rut depth from the previous year and the lane width. A summary of the data used can be found in Table 1 and Figure 1 and Supplementary Material ??.

Table 1.: Nomenclature and variables

Terms and Variables	Description/Value
Rut depth ($d_{i,t}$, millimetre)	Measurement for year t for all 20-metre stretch (i); mean = 12.11 millimetres and sd = 6.78 millimetres
Lane width (w_i , metre)	Half (or quarter) of width of 2-lane (or 2 – 2 lane) used; mean = 6.02 millimetres and sd = 0.69 millimetres
Pavement type	Asphalt concrete (Ac), asphalt gravel concrete (Agc) and stone mastic asphalt (Sma)
AADT (vehicles/year)	568 – 18500 vehicles, with half (or quarter) of AADT for 2-lane (or 2 – 2 lane) road used
$r_{i,t}$ (millimetre/year)	Change in rut depth between year t and $t - 1$ (for $t = 1, \dots, T$).

2.3.1. Rut depth and rutting

The rut depth is measured annually using a laser scanner device **ViaPPS** (Pavement Profile Scanner) — a measurement system developed by **ViaTech** in cooperation with NPRA (Peraka and Biligiri 2020). The annual rut depth measurement is used to calculate *rutting* (mm/year), the indicator variable used for assessing pavement performance. We denote the rut depth variable at road segment $i = 1, \dots, n$ in year t as $d_{i,t}$, and $r_{i,t}$ as *rutting* (mm/year). Rutting for year t at segment i is defined as

$$r_{i,t} = d_{i,t} - d_{i,t-1}. \quad (1)$$

In the case of repavement, rut depth is smaller the proceeding year resulting in large negative values of $r_{i,t}$. Therefore, following Vedvik (2021), large negative rutting values are removed;

$$r_{i,t} = \begin{cases} r_{i,t}, & \text{if } r_{i,t} \geq -d_{i,t}/2 \\ \text{NaN} & \text{otherwise,} \end{cases} \quad (2)$$

i.e., $r_{i,t}$ is kept if it is at least half the rut depth, or assigned NaN (not a number) otherwise. Some missing rutting data may occur due to uncertainty arising from the actual rut depth measurements or the data collection process (Figure 1, graph (b) shows large variability in rutting).

2.3.2. Annual Average Daily Traffic (AADT)

The annual average number of daily traffic (AADT) is available for each road segment for each year. AADT ranges from 568-18500 between the years 2010 – 2020, with more traffic close to Stjørdal and less towards Sweden. NPRA states that high-traffic roads have an AADT of more than 5000 vehicles and recommends maintenance at rut depth values exceeding 20 millimetres, while low-traffic roads with AADT lower than 5000 require pavement treatment when rut depth exceeds 25 millimetres. Up to 2.5 kilometres along the road, a quarter of the AADT is used in the analysis or half of the AADT otherwise. In all analyses, AADT in ten thousands are used.

2.3.3. Pavement type

In Norway, asphalt concrete is used on all types of roads and in all traffic classes. The asphalt mixtures used on the European route E14 are; asphalt concrete mixtures (**Ac**) and asphalt gravel concrete (**Agc**), and a stone mastic asphalt mixture (**Sma**). These include stone mastic asphalt **Sma** is the stronger and densely graded asphalt mass with unmodified binders and is mainly used on high-traffic roads; and asphalt concrete (**Ac**) and asphalt gravel concrete (**Agc**), which are mainly used on low-traffic roads of up to 5000 vehicles, courtyards, sidewalks and bicycle paths. These are softer, dynamic pavement mixtures, with less stringent requirements for the nature and grading of the stone material compared with that of stone mastic asphalt. Asphalt concrete, is however, more stringent than Asphalt gravel concrete; it is a dense-graded asphalt used as a protective layer over the road surface, or laid over a layer of asphalt gravel concrete (d’Angelo *et al.* 2008, vegvesen Vegdirektoratet 2009, Taddesse 2013, Zhang *et al.* 2022).

2.3.4. Lane width

The road width is quite variable and depends on the number of lanes. Since one lane is considered for the purposes of analysis, a quarter of the measured width up to 2.5 kilometres from Stjørdal or half of the measured width for the rest of the road stretch is used.

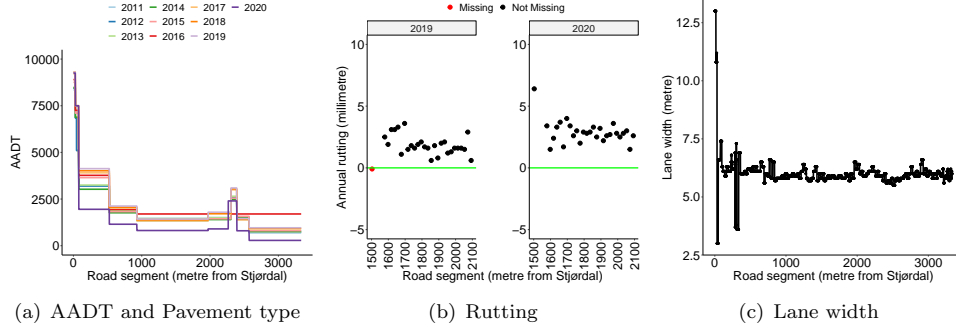


Figure 1.: AADT together with pavement type (a), rutting (for years 2019-2020, mm/year — missing in red) (b), lane width (metre) (c).

2.4. Exploratory analysis of rutting

On average, over all stretches and years, rutting is 1.67 mm/year; see Figure 2 (a). The density plots, 2 graph (b), show rutting for all segments for each year. Some years having higher rutting levels and are more widely distributed than others. The lines in graph (c) gives the correlation of rutting values with respect to distance (mean across all years, and two randomly selected years; 2011 and 2013) (Bachmaier and Backes 2011). It is computed from the observed rutting and shows how the rutting values are correlated with respect to distance between the corresponding segments. The distance (metre) is shown on the x-axis, and the calculated correlation between rutting values is on the y-axis. The graph shows some spatial dependencies of pavement rutting along the road. These exist for short distances of up to (\sim) 300 metres (3 kilometres).

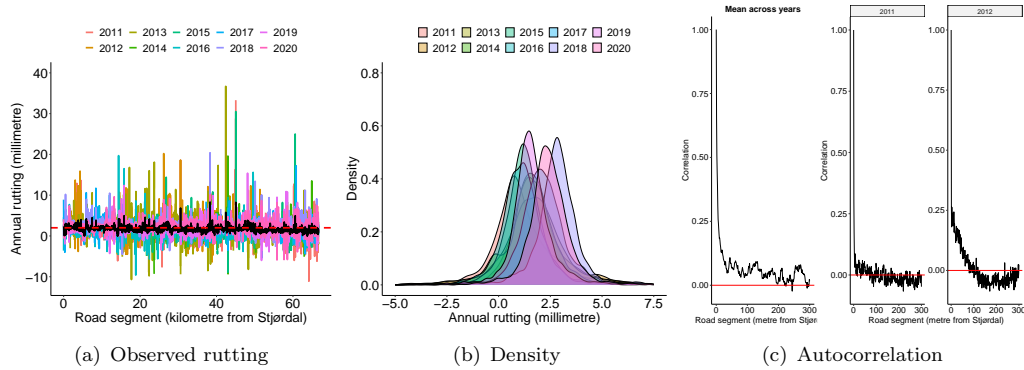


Figure 2.: Graph (a): Observed rutting for each year (2011-2020), observed mean rutting 1.67 mm/year (■ ■ ■ ■), and the observed mean rutting across segments (—). Graph (b): Rutting density plots, graph. Graph (c) shows how rutting values are correlated with distance. Spatial dependencies in rutting exist up to 3 kilometres.

3. Latent Gaussian models for Rutting

A Bayesian latent Gaussian model is a three-stage hierarchical model consisting of a likelihood, a latent Gaussian field, and hyperparameters. In this paper, the true rutting observations $\mathbf{r} = (r_1, \dots, r_n)$ at location $i = 1, 2, \dots, n$ in year t is modelled

as a latent Gaussian field, assumed to have a Gaussian prior with zero mean and a small number of hyperparameters (< 15). We specify six (6) models with different explanatory variables included and with and without spatial and random effects.

3.1. Latent field: model for true rutting

We denote the observed rutting for segment i in year t as $r_{i,t}$. Let $\eta_t(s_i)$ denote the true rutting at location s_i . We model the observed rutting as Gaussian with expected value $\eta_t(s_i)$ and variance σ_ε^2 . Hence, σ_ε^2 is the uncertainty of the Gaussian observations. The unstructured error terms $\varepsilon_{i,t} \stackrel{i.i.d.}{\sim} \text{Normal}(0, \sigma_\varepsilon^2)$ are independent and identically distributed (i.i.d). Further, $r_{i,t}$ is conditionally independent, given the latent field $\eta_t(s_i)$.

3.1.1. Likelihood: observed rutting given true rutting

We first model the observed rutting, given the true rutting. This is referred to as the likelihood model in the Bayesian hierarchical model setting. The likelihood of the rutting, $r_{i,t}$, at road segment $i = 1, \dots, n$ in year $t = 1, \dots, T$ is expressed as

$$r_{i,t} \mid \eta_t(s_i) \sim N(\eta_t(s_i), \sigma_\varepsilon^2). \quad (3)$$

We only consider models that have an interaction with AADT, and include a random yearly effect. It is known that more traffic gives more rutting, so we include traffic (AADT) in the model as an interaction with each of the explanatory variables. This means that for pavement type, we assume that the rutting is linear for all pavement types (double traffic means double rutting), but that the different pavement types can have different rates of deterioration. From the explanatory analysis (Figure 2), we found that the rutting seems to be on different levels for different years, and this might be explained by different weather conditions. To account for this, we include a random yearly effect in the model.

3.1.2. Non-spatial rutting model: based on explanatory variables and year effect

The model without spatial effects (non-spatial) has the linear predictor

$$\eta_t(s) = \beta_{Ac} z_{Ac(s,t)} + \beta_{Agc} z_{Agc(s,t)} + \beta_{Sma} z_{Sma(s,t)} + \beta_{d-1} z_{d-1(s,t)} + \beta_w z_w(s,t) + \gamma_t. \quad (4)$$

The model assumes that the level of expected rutting (mm/year) is influenced by an interaction effect of the annual average daily traffic (AADT) and some explanatory variables, including the level of rut depth from the previous year (z_{d-1}), the lane width (z_w) and pavement type. Technically, $z_{Ac}(s, t)$ is

$$\begin{cases} \text{AADT (in ten thousands) if pavement at } (s, t) \text{ is Ac,} \\ 0 \text{ if not Ac;} \end{cases}$$

similarly, for pavement types Agc and Sma, representing asphalt gravel concrete and stone mastic asphalt, respectively. The effect of lane width, say, on rutting is dependent

on the traffic intensity. The random yearly effect is assumed to be distributed as $\gamma = (\gamma_1, \gamma_2, \dots, \gamma_T) \sim \text{Normal}(\mathbf{0}_T, \tau_\gamma^{-1})$.

3.1.3. Model including spatial effects

There are several variables not included in our model (Equation (4)) that are known to influence rutting. Examples are variables related to weather, bearing capacity and proportion of heavy traffic load. Most of these variables are spatially dependent, and segments close in space are likely to be more similar than segments further apart. This can be accounted for and utilised by including spatial random effects. The spatial random effect is a Gaussian process (GP) along the road and can be interpreted as the part of the residual (the part of the model not explained by the explanatory variables; lane width, rut depth from the previous year and pavement type) that is spatially dependent. Further, it is reasonable that some of the spatial random effect is consistent over years (e.g., bearing capacity, side slope height, surface and base curvature and proportion of heavy traffic) while others vary between years (e.g., heavy rain events or more heavy traffic due to construction work). Therefore, we include both an annually varying spatial process $\xi_t(\mathbf{s})$ for year $t = 1, \dots, T$, and a common spatial process $\omega(\mathbf{s})$, which we refer to as the spatial rutting component (Ingebrigtsen *et al.* 2015). The spatial rutting component is the spatial contribution to the total rutting that is not explained by the other variables e.g., variables in the non-spatial model in Equation (4). This contribution can either be positive or negative, depending on the other variables and either over- or underestimate the observed rutting. The linear predictor for the model including spatial effects is described as

$$\eta_t(\mathbf{s}) = \beta_{Ac} z_{Ac(s,t)} + \beta_{Agc} z_{Agc(s,t)} + \beta_{Sma} z_{Sma(s,t)} + \beta_{d-1} z_{d-1(s,t)} + \beta_w z_w(s,t) + \gamma_t + \xi_t(\mathbf{s}) + \omega(\mathbf{s}), \quad (5)$$

where the remaining model parameters are defined as that in Equation 4.

The common spatial process $\omega(\mathbf{s})$ in Equations (5) is the time constant variable that can give rutting not explained by known variables (or unexplained rutting). It is a Gaussian random process $\{\omega(\mathbf{s}) : \mathbf{s} \in \mathcal{D} \subseteq \mathbb{R}^d\}$ such that for any $n \geq 1$ and for each set of spatial locations (s_1, \dots, s_n) satisfies

$$\omega(\mathbf{s}) = \{\omega(s_1), \dots, \omega(s_n)\} = (\omega_1, \dots, \omega_n) \sim \text{Normal}(\boldsymbol{\mu}^\omega, \Sigma^\omega), \quad (6)$$

where $\boldsymbol{\mu}^\omega = \{\mu^\omega(s_1), \dots, \mu^\omega(s_n)\}$ is the mean vector and $\Sigma_{ij}^\omega = \text{Cov}\{\omega(s_i), \omega(s_j)\} = C^\omega\{\omega(s_i), \omega(s_j)\}$ are the elements of the covariance matrix defined by the Matérn stationary isotropic covariance function. Simply, this covariance is expressed as $C^\omega(d; \sigma_\omega^2, \rho_\omega)$, where $d = \|s_i - s_j\|$ is the distance between two road segments; σ_ω^2 is the marginal variance of the spatial rutting component and ρ_ω is the spatial range for the spatial rutting component. These are the parameters to be estimated.

Similarly for the annually varying spatial field $\xi_t(\mathbf{s})$, the parameters to be estimated are $\sigma_{\xi_t}^2$ and ρ_t . This can be done following the approach as in Equation 6. Detail description of the Matérn covariance structure is found in (e.g., Blangiardo and Cameletti 2015, Krainski *et al.* 2018) and the Supplementary Material ??.

3.1.4. Other models for comparison

We consider simpler non-spatial and spatial models for comparison. These models include some of the known explanatory variables and are presented in Table 2. The most complex spatial model (in Equation 5) we refer to as **Model 1**, and its non-spatial version, Equation (4), as **Model 4**. These models include three explanatory variables.

Table 2.: Statistical models fitted

NAME	MODEL DESCRIPTION
SPATIAL	
Model 1	$\eta_t(s) = \beta_{Ac}z_{Ac}(s,t) + \beta_{Agc}z_{Agc}(s,t) + \beta_{Sma}z_{Sma}(s,t) + \beta_{d-1}z_{d-1}(s,t) + \beta_w z_w(s,t) + \gamma_t + \xi_t(s) + \omega(s)$
Model 2	$\eta_t(s) = \beta_{Ac}z_{Ac}(s,t) + \beta_{Agc}z_{Agc}(s,t) + \beta_{Sma}z_{Sma}(s,t) + \beta_{d-1}z_{d-1}(s,t) + \gamma_t + \xi_t(s) + \omega(s)$
Model 3	$\eta_t(s) = \beta_{Ac}z_{Ac}(s,t) + \beta_{Agc}z_{Agc}(s,t) + \beta_{Sma}z_{Sma}(s,t) + \gamma_t + \xi_t(s) + \omega(s)$
NON-SPATIAL	
Model 4	$\eta_t(s) = \beta_{Ac}z_{Ac}(s,t) + \beta_{Agc}z_{Agc}(s,t) + \beta_{Sma}z_{Sma}(s,t) + \beta_{d-1}z_{d-1}(s,t) + \beta_w z_w(s,t) + \gamma_t$
Model 5	$\eta_t(s) = \beta_{Ac}z_{Ac}(s,t) + \beta_{Agc}z_{Agc}(s,t) + \beta_{Sma}z_{Sma}(s,t) + \beta_{d-1}z_{d-1}(s,t) + \gamma_t$
Model 6	$\eta_t(s) = \beta_{Ac}z_{Ac}(s,t) + \beta_{Agc}z_{Agc}(s,t) + \beta_{Sma}z_{Sma}(s,t) + \gamma_t$

3.2. Prior models

The priors on the explanatory variables $\beta = (\beta_{Ac}, \beta_{Agc}, \beta_{Sma}, \beta_{d-1}, \beta_w)$; and the hyperparameters for the random yearly effect γ are assumed as follows

$$\begin{cases} \beta \stackrel{i.i.d}{\sim} \text{Normal}(0, 0.001^{-1}) \\ \tau_\gamma \sim \text{Gamma}(0, 5 \cdot 10^{-5}) \\ \sigma_\varepsilon \sim \text{Gamma}(0, 5 \cdot 10^{-5}). \end{cases}$$

Vague priors are used, and we let the data inform about the parameters to be estimated. The random yearly effect is evident in density plots in Figure 2 (c), which shows the varying yearly effect of rutting. For easier interpretations, the priors for the spatial components $\xi_t(s)$ and $\omega(s)$ are set through the spatial range ρ and marginal standard deviation $\sigma_\omega(s)$ of the GRFs with Matérn covariance function in Equation (??). These are acquired jointly following the penalized complexity (PC) framework (Simpson *et al.* 2017, Fuglstad *et al.* 2019). The prior for the range is set through the probability $\Pr(\rho < 250) = 0.15$, indicating that there is a 15 percent probability that the spatial range is less than 250 metres. For the marginal standard deviation, the prior is set through the probability $\Pr(\sigma_{\omega(s)} > 2.5) = 0.05$, indicating that there is a 5 percent probability that the marginal standard deviation for the rutting is over 2.5 meters. These priors are the same for all the spatial fields.

3.3. Inference and implementation

In Bayesian statistics, inference is done by computing posterior distributions for the parameters of interest based on prior models (Section 3.2), the likelihood model in Equation (3) and the data. Our goal is to estimate the marginal posteriors of the spatial rutting component, the regression coefficients, the hyperparameters and the expected rutting (marginal likelihood), given the known explanatory variables. We use INLA (integrated nested Laplace approximation) (Rue *et al.* 2009a, 2017, Martino

and Riebler 2019), which is implemented in the R package R-INLA to approximate these marginal distributions.

3.4. Model evaluation

Three model fit measures are available; the deviance Information Criterion (DIC) (Spiegelhalter *et al.* 2002), the Watanabe-Akaike Information criterion (WAIC) (Watanabe and Opper 2010, Gelman *et al.* 2014) and the log-likelihood (Hubin and Storvik 2016) can be obtained for each of them in order to select the best one. The DIC and WAIC are based on hierarchical modeling generalizations of the Akaike Information Criterion (Akaike 1974), and are widely used in Bayesian statistics to perform model comparison. The values are determined by the model fit and its complexity, and by a penalty applied for overfitting. Models with a high level of complexity and a high goodness-of-fit, and models with the lowest DIC and WAIC should be chosen.

4. Results and discussion

We fit the models in Section 3.1.4 to the data in Section 2.3. For interpretability, the explanatory variables are standardized by subtracting the mean and dividing by the standard deviation.

The results from the spatial Model 1 and the non-spatial version Model 4 are used to demonstrate the models' performance. Based on Model evaluation criteria (Table A2), the spatial and non-spatial models with more explanatory variables (Model 1, 3 or 4) are selected as the best model, with the highest goodness-of-fit (lowest DIC and WAIC). While Models 3 or 5 capture the random (and/or spatial) variability of pavement rutting, they do not necessarily explain more of the uncertainty. Therefore, the spatial and non-spatial Models 1 and 4 are considered the most appropriate model to infer pavement performance from rutting data and are used for further analysis. The results for the remaining models are given in Appendix A.

4.1. Estimated spatial rutting component

Using Model 1 and the estimates obtained from fitting this model, we can identify areas with high rutting rates that are not explained by known factors such as pavement type or lane width. This is given by the posterior mean of the spatial rutting component $\omega(s)$. The spatial rutting component $\hat{\omega}(s)$ is plotted in Figure 3.

We find that the rutting inferred from $\hat{\omega}(s)$ is quite variable along the road; graph (a). The mean unexplained rutting contribution from $\hat{\omega}(s)$ is 0.01 mm/year and the maximum unexplained portion is 3.21 mm/year. This means that some locations would have 3.21 mm/year extra rutting compared with the mean. There are also several locations where rutting exceeds 2 mm/year (the observed mean rutting is 1.67 mm/year; see Figure 2, graph (a)). This suggests that there are unexplained or unaccounted influential factors of rutting in a given year, one of which could be the weather. Rutting of at least 2 millimetres at some locations (upper panel), or in a given year (lower panel), is concerning, given the expected lifetime of the pavement and the recommended levels for treatment. If maintenance is to be carried out at 20 – 25 millimetres rut depth levels, depending on traffic, and pavement designs are expected to last between 20 – 30 years, then some parts of the road would survive at most 12.5 years (10 years in high-traffic areas). The minimum unexplained portion of rutting from $\hat{\omega}(s)$ is -1.72 mm/year. This suggests that those locations would have 1.72 mm/year less

rutting compared with mean (0.01 mm/year). That is, better real-life rutting performance than expected by the model. The rutting from the spatial component do appear to be relatively systematic, with a difference between the highest and lowest rutting values of 4.93 millimetres.

Including spatial components in the model allow us to explain more of the rutting variability and identify areas with high rutting rates not explained by known variables. This is confirmed in Figure 3 (b), where the rutting explained by the random yearly effect from the spatial model is at least 0.5 mm/year less compared with the non-spatial model. We further investigate locations with unexpectedly high rutting rates in Section 4.2.

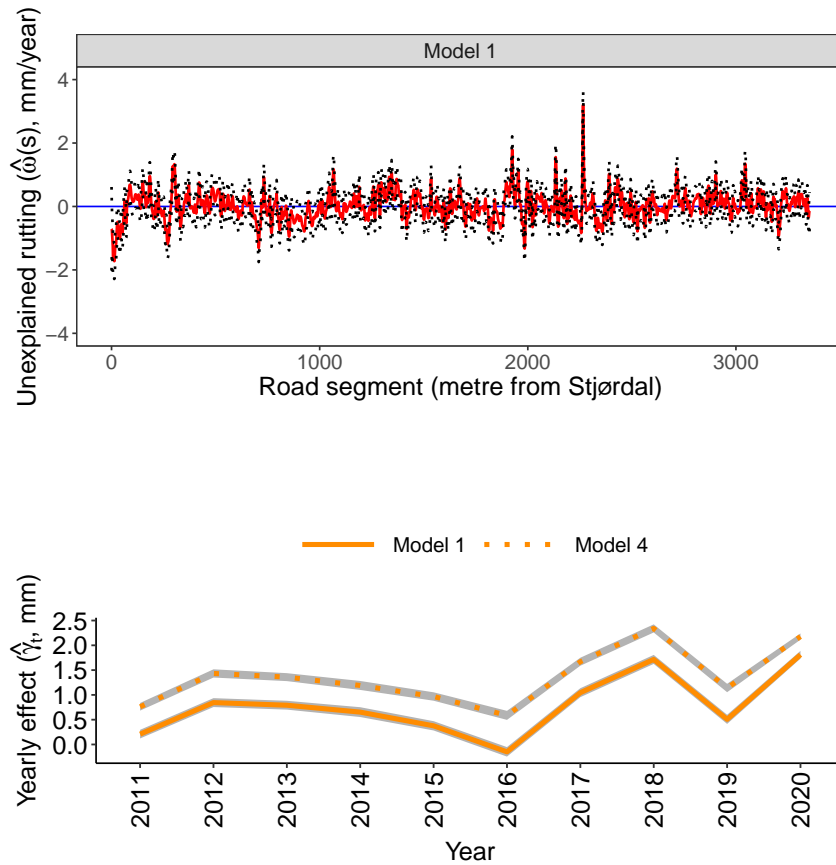


Figure 3.: Upper panel: Spatial rutting component (or unexplained portion of rutting $\{\hat{\omega}(s)\}$), with approximate 95% credible interval. Lower panel: Rutting from the random yearly effect ($\hat{\gamma}_t$) from Model 1 (—) and Model 4 (⋯), with approximate 95 % credible interval.

4.2. *Estimated rutting from the explanatory variables, random yearly effect and spatial rutting component*

We can also use the spatial model (Model 1) to identify locations, termed ‘hot spots’, that are in the greatest need of maintenance (Figure 4). For illustration, the model

is used to infer rutting from the coefficients of the explanatory variables $\hat{\beta}$; the mean of the posterior means of the random yearly effects $\hat{\gamma}$; and the posterior mean of the spatial rutting component $\hat{\omega}(s)$. This is both the explained and unexplained rutting. The random yearly effect γ_t varies from year to year, so we use an estimate of the mean, i.e., $\hat{\gamma}$. In addition, $\hat{\sigma}_{\xi_t}$ varies annually, but it is quite small (see Supplementary Materials ??) so it is not considered in our illustration.

First, we estimate the rutting from the sum of the coefficients of the explanatory variables and the mean of the posterior means of the random yearly effects $\hat{\gamma}$ only. The results are from Model 1, so we denote this by: $\hat{\eta}^* = \hat{\beta}_{(1)}z_{(1)(s,t)} + \hat{\gamma}$. Next, we estimate the rutting from the sum of the coefficients of the explanatory variables, the mean of the random yearly effect $\hat{\gamma}$, and posterior mean of the spatial rutting component $\hat{\omega}(s)$; we denote by $\hat{\eta} = \hat{\beta}_{(1)}z_{(1)(s,t)} + \hat{\gamma} + \hat{\omega}(s)$. Since the different asphalt types; stone mastic asphalt (Sma), asphalt concrete (Ac) and asphalt gravel concrete (Agc), are laid at specific locations along E14, these are highlighted in various colours along the plot line $\hat{\eta}^*$. These results are shown in Figure 4.

The effect of pavement type on rutting (i.e., the line showing the three asphalt types; Sma, Ac and Agc) is much less variable (ranging from 0.96 to 3.89 mm/year) compared with the sum of the explanatory variables, the mean of random yearly effect and the spatial rutting component (ranging from 0.03 to 4.68 mm/year); see graph (a). This suggests that the explanatory variables and the random yearly effect alone do not capture or realistically represent the variability in the expected rutting. Accounting for both spatial and random yearly effects allow more of the rutting variability to be explained. These can be seen in Table 3 and Table A1 in Appendix A, where $\hat{\sigma}_{\omega}(s)$ explains 0.47 and $\hat{\gamma}$ explains 0.72 compared with the remaining uncertainty ($\hat{\sigma}_{\varepsilon} = 1.38$) from the spatial model and the non-spatial version ($\hat{\sigma}_{\varepsilon} = 1.54$). Additionally, the expected lifetime at some sections of the pavement is at most 6 years considering only the explanatory variables and the random yearly effect or 5 years considering the spatial rutting component $\hat{\omega}(s)$. This expected lifetime is depended upon traffic (i.e., 20 or 25 millimetres recommended maintenance for high- or low-traffic areas). We also see that the expected rutting $\hat{\eta}$ can be high, where the rutting is explained by the explanatory variables; or it could be moderate, but the spatial rutting component $\hat{\omega}(s)$ is large. Compared with the observed mean rutting across segments, which ranges from -0.05 to 8.33 mm/year (see Figure 2, graph (a)), the maximum expected rutting estimated from the model (i.e., 4.68 mm/year) is approximately halved the maximum of the observed mean rutting.

In graph (b), the expected rutting from the sum of the explanatory variables, the random yearly effect and the spatial rutting component; lane width; and AADT (per ten thousand) are plotted for a short section of the road. This part of the road, from segments 1500 – 2700 (or 30000 – 54000 metres towards Sweden), is dominated by the weaker pavement type Agc and, as shown in graph (a), has spikes of accelerated rutting. When plotted against the AADT or lane width, we see that rutting is higher with increasing traffic and narrow road lanes. This large variability may, presumably, be a result of: (i) a change in asphalt type from asphalt concrete (Ac) to asphalt gravel concrete (Agc, see same road stretch in the graph (a)); (ii) the type of traffic in that area, e.g., heavy-traffic (vehicles > 3500 kilograms); (iii) poor road design; or (iv) lack of timely and efficient pavement rehabilitation.

The observed mean rutting (Figure 2 (a) in Section 2.4) is estimated to be 1.67 mm/year. From graph (a), we found that the expected rutting, $\hat{\eta}$, for 351 road segments exceed this mean, and 22 of these road segments gave estimated rutting that exceeds 3 mm/year (graphs (c) and (d), respectively). These 22 locations suggest potential hot

spots for accelerated rutting and would require urgent maintenance as the expected lifetime would be at most 8 years, depending on traffic.

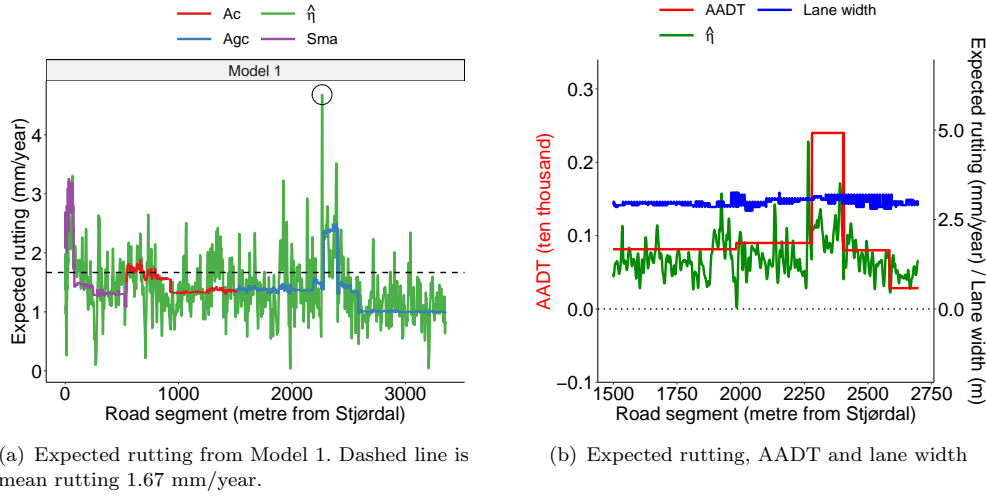
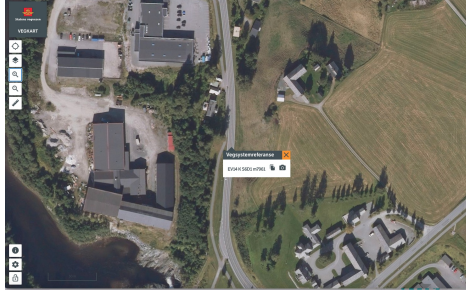


Figure 4.: Graph (a): Expected rutting from: i) the spatial rutting component $\hat{\omega}(s)$, the random yearly effects plus coefficients of all explanatory variables, interacting with AADT for Model 1 $\{\hat{\eta}\}$ and ii) from the sum of the explanatory variables and the of random yearly effect only $\{\hat{\eta}^*\}$, with each asphalt type highlighted. The effects are inferred for the year 2020. Graph (b): Expected rutting plotted against AADT and lane width for a small stretch of E14 (closer to Sweden). Graphs (c) and (d) give the locations where rutting exceeds 2 mm/year or 3 mm/year, respectively.

4.2.1. Investigating areas with high rutting rates

The large spike in Figure (4) (a), showing high rutting rates, is further investigated. We look at the road segments 2100 - 2500 metres surrounding this spike. This area is the municipality of Meråker, just 20 kilometres west of Storlien. This stretch, as shown in Figure 4 (a), gave high expected rutting, reaching 4.68 millimetres, with an expected lifetime of just 5 years (low-traffic area with required maintenance at 25 millimetres rut depth). This accelerated rutting could be because of clogged drainage, flooding, missing side ditches (Figure 5), heavy-traffic or road designs with railguards

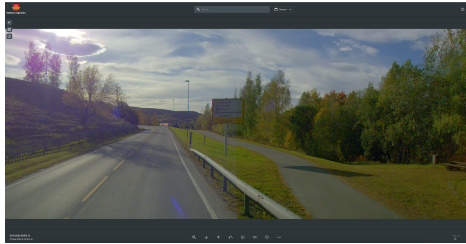
installed close to the lane edge, allowing that traffic drives more within the same wheel tracks. Meråker has industry and agriculture, therefore, roadways are more subjected to heavy vehicles, including farm vehicles such as tractors (industry, wheel drive, row crop).



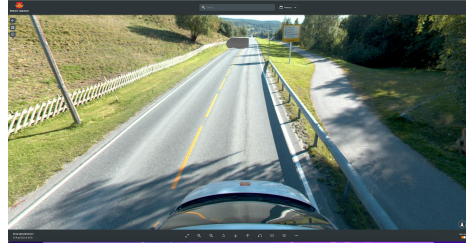
(a) Short section between EV14 S6D1 m6148-m8212 F1 with high rutting.



(b) Location EV14 S6D1 m8017 F1 in year 2020



(c) Location EV14 S6D1 m7971 F1 in year 2021

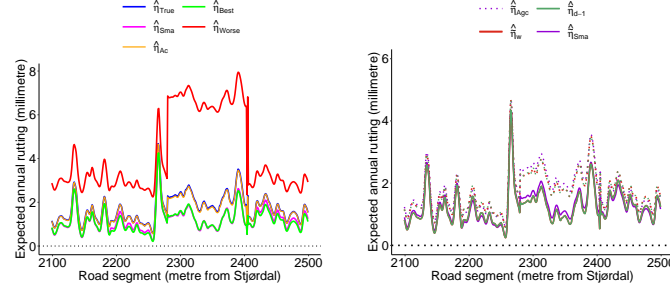


(d) Location EV14 S6D1 m7961 F1 in year 2022

Figure 5.: Graph (a): Location with high rutting rates (road segments 2100 – 2500 towards Sweden). Graphs (b), (c) and (d) show the location, in years 2020-2022 (see Statens vegvesen or go to the next url: <https://vegkart.atlas.vegvesen.no/#kartlag:nib/@337286,7036109,14/vegsystemreferanse:337312.447:7036064.784>)

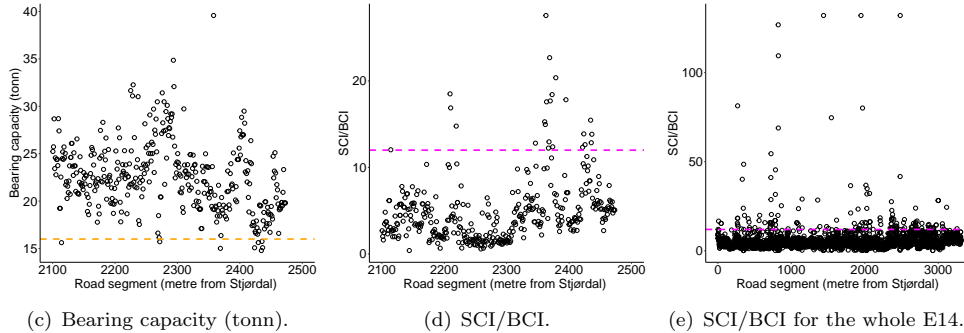
To further investigate this road section with high rutting values, we consider the effect of the explanatory variables, random yearly effect, and the spatial rutting component. We explore the spatial Model 1 using various values of the explanatory variables to approximate the rutting. First, we use the true values in the data, i.e., the asphalt type, the lane width and rut depth measured at that location, denoted by $\hat{\eta}_{\text{True}}$. Second, the asphalt type is changed from its true state of asphalt gravel concrete (Agc) to asphalt concrete (Ac) or stone mastic asphalt (Sma); represented by $\hat{\eta}_{\text{Ac}}$ or $\hat{\eta}_{\text{Sma}}$, respectively. Third, the ‘best’ (or ‘worse’) values are used, i.e., if pavement type with the strongest binder, Sma, or a rut depth value from the previous year of 0.01 millimetres (~ 0), or lane width of 6 metres were used. This is denoted by $\hat{\eta}_{\text{Best}}$. These values are chosen following the reasoning: (\sim) zero rut depth means no rutting; wider roads mean a slower rate of rutting. The values considered to be ‘worse’, resulting in accelerated rutting, include a rut depth from the previous year of 25 millimetres, lane width of 2.75 metres and asphalt gravel concrete (Agc) pavement type. This is denoted by $\hat{\eta}_{\text{Worse}}$. These values are found in the E14 data set. The cases are plotted in Figure 6 (a), which gives the expected rutting from the sum of the explanatory variables, the yearly random effect $\hat{\gamma}$ and the spatial rutting component $\hat{\omega}(s)$.

Using the worse values in the analysis, the expected rutting is at least 2.3 (2.25 – 7.94) mm/year; Figure 6, graph (a) (—). This means that with low AADT and the recommended maintenance rut depth level of 25 millimetres, pavement deterioration would accelerate and treatment or new pavement would be required within 3 to 11 years after initial construction. The best covariate values (—) gave at most 4.26 mm/year of rutting, with the least rutting value (0.21 mm/year). And, the earliest maintenance activity would be required from around 6 years after construction or maintenance. Further, the best values (—) gave similar estimates of annual rutting to that of using the stronger asphalt binder type Sma (stone mastic asphalt, —), except at road segments 2279 – 2388, where the estimated rutting from only changing the asphalt type from asphalt gravel concrete to stone mastic is lower than that of using the best values. This suggests that asphalt type is the driving factor of expected rutting. Pavement types asphalt gravel concrete (Agc, —) and asphalt concrete (Ac, —) gave similar estimates of expected rutting. This result is expected because they are made with similar binder concentration strengths.



(a) Expected rutting at road segments 2100 – 2500 (metres) towards Sweden.

(b) Expected rutting from adding each explanatory variable added sequentially.



(c) Bearing capacity (tonn).

(d) SCI/BCI.

(e) SCI/BCI for the whole E14.

Figure 6.: Graph (a): Expected rutting inferred from the spatial rutting component $\hat{\omega}(s)$ plus the ‘best’ (or ‘worse’) explanatory values at road segments 2100 – 2500 towards Sweden. The estimate $\hat{\eta}_{\text{Agc}}$ is for pavement type Agc plus the random yearly effect and the spatial rutting component. Graph (b): expected rutting inferred from $\hat{\omega}(s)$ plus the random yearly effect $\hat{\gamma}$ and each explanatory variable added sequentially in the model. Graph (c): bearing capacity for year 2021 (tonn), with 16 tonn or greater indicating a good parameter. Graphs (d) and (e) give the ratios of surface curvature index (SCI) to base curvature index (BCI) for road segments 2100-2500 (metres) or the whole E14, respectively, with values below 12 indicating a good curvature index.

The above results suggest pavement type as the driving explanatory variable for expected rutting (Figure 6), so we determine its importance on rutting by changing the asphalt type from the true one (i.e., asphalt gravel concrete, Agc) to the stronger asphalt type Sma (stone mastic asphalt) and keeping all other variables (e.g., lane width) as given in the data set. The remaining explanatory variables are then added sequentially in the model with pavement type, i.e., stacking. Pavement type (Agc or Sma) is first added to the random yearly effect $\hat{\gamma}$ and the spatial rutting component $\hat{\omega}(s)$. We denote this by: $\hat{\eta}_{\text{Agc}} = \hat{\beta}_{\text{Agc}} z_{\text{Agc}(s,t)} + \hat{\gamma} + \hat{\omega}(s)$ or $\hat{\eta}_{\text{Sma}} = \hat{\beta}_{\text{Sma}} z_{\text{Agc}(s,t)} + \hat{\gamma} + \hat{\omega}(s)$, respectively. Next, rut depth from the previous year is added, and it is represented as $\hat{\eta}_{d-1} = \hat{\beta}_{\text{Agc}} z_{\text{Agc}(s,t)} + \hat{\beta}_{d-1} z_{d-1}(s,t) + \hat{\gamma} + \hat{\omega}(s)$ or $\hat{\eta}_{d-1} = \hat{\beta}_{\text{Sma}} z_{\text{Sma}(s,t)} + \hat{\beta}_{d-1} z_{d-1}(s,t) + \hat{\gamma} + \hat{\omega}(s)$. Similarly, the model with lane width $\{\hat{\beta}_w z_{w(s,t)}\}$ added is represented by $\hat{\eta}_w$. The results are shown in Figure 6, graph (b).

Results from using stone mastic asphalt (Sma) are represented by the solid lines, and from using asphalt gravel concrete (Agc), the dotted lines. The results confirm that pavement type is the driving factor of rutting. If the stronger binder type Sma were laid at this stretch instead of the true pavement type Agc, expected rutting would decrease, reaching at most 4.35 mm/year (compared with 4.68 mm/year). This is approximately 0.33 mm/year less rutting annually, with an expected lifetime of 6 years, i.e., 1 extra year.

We also look at the available data for bearing capacity (Figure 6, graph (c)), surface curvature index (SCI) and base curvature index (BCI) for road segments 2100-2500. The data is available for year 2021, but it is a good indicator of the construction quality and the soil to sustain pressure over the past decade; Figure 6, graph (c). For bearing capacity, values greater than 16 tonns (••••) suggest a good foundation design. The ratio of SCI to BCI ((Figure 6, graphs (d) and (e)) gives an indication of the location of the deflection (deformation) in the pavement layer (surface or base). The data suggests good bearing capacity, and that high rutting may be a result of other influential factors, e.g., side slope height (data not available), lack of side ditches to effect water drainage or deformation in the sub-base layer developed in thawing periods. We note that the bearing capacity data was sampled during the summer and corrected for temperature. During the summer, the measurements can be higher due to dry conditions, compared to those in thawing periods with high moisture content. Permanent deformation could have occurred during thawing periods, resulting in high rutting. There is also the possibility of varying construction material quality at various parts of the road, even though the pavement type (asphalt gravel concrete) is the same for the entire stretch (road segments 1500 – 3355). Therefore, we investigate the consistency in the pavement construction by looking at deflections in the surface layer and the subsoil or reinforcement layer. The ratio of SCI to BCI is a good indication of the strengths or weaknesses in the construction, with SCI/BCI < 12 (••••) indicating a good parameter value. If this ratio is constant, then the construction is considered even, otherwise, there are variations indicating deformation in the various layers. The data, suggests an uneven construction of E14, with deeper deflections in the base layer.

We conclude that pavement type is the most important contributing factor to rutting. So, stronger binder types are recommended to ensure longer expected lifetimes.

4.3. *Estimated model parameters*

The estimated parameters and 95% credible intervals (CI) for the spatial Model 1 and non-spatial Model 4 are reported in Table 3. Comparing the coefficients for the ex-

planatory variables between spatial models and their non-spatial version, we observe that the spatial models have considerably larger estimates for the regression coefficients of pavement type (see also Figure A.1 in Appendix A). Further, we see that the variance of the ‘noise’ term ($\hat{\sigma}_\varepsilon$) is larger for the models without the spatial rutting component. One explanation for this result is that the spatial rutting component account for unobservable factors, e.g., weather that vary in space, the effect of studded tires and other influencing factors such as traffic type that are not included in the model. Varying weather patterns across Norway and towards the Swedish border will affect the function of surface layers of pavement construction. In the winter time, increased temperatures result in a shorter time of frozen ground and snow on the surface and changes in the number of freeze-thaw cycles, thus, negatively affecting lower-grade binder types such as asphalt gravel concrete (Agc) and leading to increasing rutting. Asphalt gravel concrete is laid from (\sim) 30 kilometres towards the Swedish border (Figure 1 (a)); an area that lie in the sub-arctic climate zone with long severe winters and short warm to cool summers Peel *et al.* (2007), Ketzler *et al.* (2021), and having poorly developed networks (rural E14 highway west of Östersund) Jenelius (2010). This area is also more likely to be traversed by heavy-traffic (exceeding 3500 kilograms or 3.5 tonnes) Hovi *et al.* (2018), Pinchasik *et al.* (2020), negatively affecting pavement performance. More of the expected rutting is also explained by rut depth and lane width from the spatial model compared with the non-spatial model. This can be seen by the smaller values of the ‘noise’ terms ($\hat{\sigma}_\varepsilon$) and uncertainty in the random year effect ($\hat{\sigma}_\gamma$) from the spatial model (see Table 3 and Table A1 in Appendix A for the simpler models).

Table 3.: Estimated model parameters with 95% credible intervals

	Spatial Model		Non-spatial Model	
	Model 1		Model 4	
	Mean/Median	95% CI	Mean/Median	95% CI
$\hat{\beta}_{Ac}$	7.13	[6.62, 7.65]	3.25	[2.81, 3.68]
$\hat{\beta}_{Agc}$	7.34	[6.92, 7.76]	3.21	[2.75, 3.67]
$\hat{\beta}_{Sma}$	3.63	[3.37, 3.90]	2.00	[1.81, 2.19]
$\hat{\beta}_{d-1}$	0.74	[0.66, 0.82]	1.08	[0.98, 1.18]
$\hat{\beta}_w$	-0.10	[-0.14, -0.07]	0.05	[-0.02, 0.11]
$\hat{\sigma}_{\omega(s)}$	0.47	[0.44, 0.51]	-	-
$\hat{\sigma}_\gamma$	0.72	[0.62, 0.88]	1.38	[0.96, 2.16]
$\hat{\sigma}_\varepsilon$	1.38	[1.38, 1.39]	1.54	[1.53, 1.56]

4.3.1. Effects of the explanatory variables

Interacting with the AADT, which is spatially varying, the effect of asphalt concrete ($\hat{\beta}_{Ac}$) and asphalt gravel concrete ($\hat{\beta}_{Agc}$) on rutting may be explained by: heavy-traffic (> 3.5 tonnes), whose proportion changes along the road and poor network design as these are constant in time. Also, various parts of the pavement have several layers due to non-removal during maintenance, leading to variability in pavement performance. The uncertainty from asphalt concrete and asphalt gravel concrete ($\hat{\beta}_{Agc}$) are also larger (wider 95% credible interval) compared with stone mastic asphalt ($\hat{\beta}_{Sma}$), but accounting for spatial dependencies allows more of the variance to be explained. Rut

depth from the previous year ($\hat{\beta}_{d-1}$) becomes more important when the spatial variability in pavement rutting is not considered (Model 4, Table 3). Further, instead of explaining the variability in expected rutting by pavement type, the non-spatial models explain this variability between years (Table 3 and Figure 3 (b)). The estimated effect of lane width ($\hat{\beta}_w$) is small and negative. This suggests that narrower lane widths would give higher expected rutting.

Based on these results, we conclude that changes in the coefficients are large when spatial dependencies of factors that are not modelled because of non-observable data (e.g., weather) are considered. And, the uncertainty explained is greater (smaller $\hat{\sigma}_\varepsilon$) for the spatial model.

5. How road authorities can make use of this model

The spatial-statistical model serves as a potent tool for road authorities, offering a data-driven approach to enhance maintenance strategies, identify critical areas for intervention and optimize road infrastructure durability. This approach facilitates a more ultimate diagnosis of rutting, empowering authorities to make informed decisions for sustainable road infrastructure.

Road authorities can use the spatial-statistical model for historical rutting data in several ways to improve maintenance strategies and prioritize interventions. These include; i) *the identification of ‘hot spots’* — the spatial model helps pinpoint hot spots where rutting is accelerating, indicating areas in urgent need of maintenance. By analyzing coefficients of factors known to influence rutting (e.g., asphalt type), random effects, and spatial components, authorities can prioritize resources for targeted interventions in these critical locations; ii) *comprehensive rutting diagnostic and understanding* — the model provides a more comprehensive diagnostic and understanding of rutting. Explanatory variables and random yearly effects alone may not capture the full variability, but the inclusion of spatial components enhances the model’s explanatory power. This comprehensive understanding allows road authorities to make informed decisions about maintenance priorities; iii) *extended expected lifetime* — considering both spatial and random yearly effects extends the expected lifetime estimation of road sections. This information is valuable for long-term planning, enabling authorities to proactively address maintenance needs and allocate resources efficiently; iv) *pavement type considerations* — the model highlights the significant impact of pavement type on rutting rates. Road authorities can use this information to make informed decisions about pavement materials during construction or rehabilitation, optimizing durability and extending the overall lifetime of the road infrastructure. The recommendation of stronger asphalt binders, such as stone mastic asphalt (Sma), to enhance pavement durability, provides practical guidance for selecting materials that contribute to longer-lasting road surfaces; v) *investigation of contributing factors* — in-depth investigations into high rutting areas reveal potential contributing factors beyond pavement type, such as drainage issues, heavy traffic, and road design flaws. Road authorities can address these factors to prevent or mitigate rutting, ensuring a more holistic approach to road maintenance; vi) *spatial model advantages* — comparisons with non-spatial models highlight the advantages of including spatial components. The larger estimates for pavement type coefficients in spatial models emphasize the importance of spatial factors in explaining rutting variations. This information reinforces the importance of using spatial models for accurate and reliable inference and predictions; and finally vii) *data-driven decision-making* — the estimated model parameters and credible in-

tervals provide a robust foundation for data-driven decision-making. Road authorities can rely on these parameters to make informed choices regarding maintenance priorities, resource allocation, and infrastructure improvements.

6. Conclusion

This research provides valuable insights into the factors influencing pavement rutting and the measurement of rut depth. The study confirms that the selection of asphalt type significantly affects rutting performance, with rut-resistant mixtures proving to be more effective in mitigating rutting. Lane width also plays a role in pavement rutting. Narrower roads tend to experience more concentrated traffic loads, which can lead to increased rutting. Wider roads, on the other hand, distribute the traffic load over a larger area, reducing the likelihood of rut formation. The data analysis indicated that narrower road stretches experienced higher rut depths. This outcome can be attributed to increased traffic volumes and higher wheel loads on roads, leading to more significant rutting. The findings, therefore, stress the importance of considering lane width when designing and maintaining pavements to minimize rutting distress. The recommendation is to incorporate a life-cycle cost-benefit perspective in the road design and planning process to minimize the potential for rutting issues over time. Further research is encouraged to explore additional factors influencing rutting; some of which include bearing capacity (Hopkins *et al.* 1998) as inadequate bearing strength of soil subgrades will not withstand construction traffic loading; ditch depth information that allows outflow of water from pavement structure; and lane width. This would likely increase the credibility of research results and the applicability of models to other road networks. In addition, it would be worthwhile to evaluate the long-term performance of rut-resistant asphalt mixtures in various traffic and environmental conditions.

Acknowledgement

The authors are grateful to Jørn Vatn and Jochen Köhler at the Norwegian University of Science and Technology for invaluable discussions on analysis and interpretation.

Disclosure Statement

The authors report no declarations of interest.

Funding

This work was supported by the Norwegian University of Science and Technology in collaboration with Statens Vegvesen Project [grant number 9056608 – SMARTere Vedlikehold (2019-2023)].

References

Akaike, H., 1974. A new look at the statistical model identification. *IEEE transactions on automatic control*, 19 (6), 716–723.

- Al-Khateeb, G. and Basheer, I., 2009. A three-stage rutting model utilising rutting performance data from the Hamburg Wheel-Tracking Device (WTD). *Road & Transport Research: A Journal of Australian and New Zealand Research and Practice*, 18 (3), 12–25.
- Alhasan, A., *et al.*, 2018. Incorporating spatial variability of pavement foundation layers stiffness in reliability-based mechanistic-empirical pavement performance prediction. *Transportation Geotechnics*, 17, 1–13.
- Bachmaier, M. and Backes, M., 2011. Variogram or semivariogram? Variance or semivariance? Allan variance or introducing a new term? *Mathematical Geosciences*, 43 (6), 735–740.
- Banerjee, S., *et al.*, 2008. Gaussian predictive process models for large spatial data sets. *Journal of the Royal Statistical Society: Series B (Statistical Methodology)*, 70 (4), 825–848.
- Blangiardo, M. and Cameletti, M., 2015. *Spatial and spatio-temporal Bayesian models with R-INLA*. John Wiley & Sons.
- Chan, C.Y., *et al.*, 2010. Investigating effects of asphalt pavement conditions on traffic accidents in Tennessee based on the pavement management system (PMS). *Journal of advanced transportation*, 44 (3), 150–161.
- Chen, D. and Mastin, N., 2016. Sigmoidal models for predicting pavement performance conditions. *Journal of Performance of Constructed Facilities*, 30 (4), 04015078.
- Cheng, C., *et al.*, 2023. Predicting Rutting Development of Pavement with Flexible Overlay Using Artificial Neural Network. *Applied Sciences*, 13 (12), 7064.
- Chou, E., *et al.*, 2008. *Pavement forecasting models*. Ohio. Dept. of Transportation.
- Chu, W., Ghahramani, Z., and Williams, C.K., 2005. Gaussian processes for ordinal regression. *Journal of machine learning research*, 6 (7).
- Dey, D.K., Ghosh, S.K., and Mallick, B.K., 2000. *Generalized linear models: A Bayesian perspective*. CRC Press.
- d’Angelo, J., *et al.*, 2008. *Warm-mix asphalt: European practice*. United States. Federal Highway Administration. Office of International Programs.
- Ebrahimi, B., *et al.*, 2019. Estimation of Norwegian asphalt surfacing lifetimes using survival analysis coupled with road spatial data. *Journal of Transportation Engineering, Part B: Pavements*, 145 (3), 04019017.
- Fuglstad, G.A., *et al.*, 2019. Constructing priors that penalize the complexity of Gaussian random fields. *Journal of the American Statistical Association*, 114 (525), 445–452.
- Gelman, A., Hwang, J., and Vehtari, A., 2014. Understanding predictive information criteria for Bayesian models. *Statistics and computing*, 24 (6), 997–1016.
- Gu, F., *et al.*, 2017. Characterization and prediction of permanent deformation properties of unbound granular materials for pavement ME design. *Construction and Building Materials*, 155, 584–592.
- Gudipudi, P.P., Underwood, B.S., and Zalgout, A., 2017. Impact of climate change on pavement structural performance in the United States. *Transportation Research Part D: Transport and Environment*, 57, 172–184.
- Gupta, A., Kumar, P., and Rastogi, R., 2014. Critical review of flexible pavement performance models. *KSCE Journal of Civil Engineering*, 18 (1), 142–148.
- Hao, W., Jian-Zhong, P., and ZHANG, J.p., 2009. Rutting law and its influence factors for asphalt pavement in long and steep longitudinal slope section. *Journal of Chang’an University: Natural Science Edition*, 29 (6), 28–31.
- Hopkins, T.C., *et al.*, 1998. *Bearing capacity analysis of pavements*. University of Kentucky Transportation Center.
- Hovi, I.B., *et al.*, 2018. Measures for reduced CO2-emissions from freight transport in the Nordic countries. *In: Proceedings from the Annual Transport Conference at Aalborg University*. vol. 25.
- Hu, A., *et al.*, 2022. A review on empirical methods of pavement performance modeling. *Construction and Building Materials*, 342, 127968.
- Hubin, A. and Storvik, G., 2016. Estimating the marginal likelihood with Integrated nested Laplace approximation (INLA). *arXiv preprint arXiv:1611.01450*.
- Ingebrigtsen, R., *et al.*, 2015. Estimation of a non-stationary model for annual precipitation

- in southern Norway using replicates of the spatial field. *Spatial Statistics*, 14, 338–364.
- Institutt, M., 2010. Ekstremvarsel. *Meteorologisk Institutt*, 12.
- Jacobson, T. and Wågberg, L.G., 2005. *Prediction models for pavement wear and associated costs*. VTI., VTI särtryck 366A.
- Jenelius, E., 2010. *Large-scale road network vulnerability analysis*. Thesis (PhD). KTH.
- Ketzler, G., Römer, W., and Beylich, A.A., 2021. The Climate of Norway. *In: Landscapes and landforms of norway*. Springer, 7–29.
- Korkiala-Tanttu, L. and Dawson, A., 2007. Relating full-scale pavement rutting to laboratory permanent deformation testing. *International Journal of Pavement Engineering*, 8 (1), 19–28.
- Krainski, E., *et al.*, 2018. *Advanced spatial modeling with stochastic partial differential equations using R and INLA*. Chapman and Hall/CRC.
- Lang, J., 2012. Comparison of pavement management in the nordic countries: Paper prepared for 4th EPAM CONFERENCE.
- Lea, J.D. and Harvey, J.T., 2015. A spatial analysis of pavement variability. *International Journal of Pavement Engineering*, 16 (3), 256–267.
- Li, L., *et al.*, 2023. A Design Method on Durable Asphalt Pavement of Flexible Base on Anti-Rutting Performance and Its Application. *Materials*, 16 (22), 7122.
- Lindgren, F. and Rue, H., 2015. Bayesian spatial modelling with R-INLA. *Journal of statistical software*, 63, 1–25.
- Lundy, J.R., *et al.*, 1992. Wheel track rutting due to studded tires. *Transportation Research Record*, 18–18.
- Martino, S. and Riebler, A., 2019. Integrated nested laplace approximations (inla). *arXiv preprint arXiv:1907.01248*.
- Pan, Y., *et al.*, 2021. A rutting-based optimum maintenance decision strategy of hot in-place recycling in semi-rigid base asphalt pavement. *Journal of Cleaner Production*, 297, 126663.
- Peel, M.C., Finlayson, B.L., and McMahon, T.A., 2007. Updated world map of the Köppen-geiger climate classification. *Hydrology and Earth System Sciences*, 11 (5), 1633–1644. Available from: <https://hess.copernicus.org/articles/11/1633/2007/>.
- Peraka, N.S.P. and Biligiri, K.P., 2020. Pavement asset management systems and technologies: A review. *Automation in Construction*, 119, 103336.
- Pérez-Acebo, H., *et al.*, 2019. Rigid pavement performance models by means of Markov Chains with half-year step time. *International Journal of Pavement Engineering*, 20 (7), 830–843.
- Pinchasik, D.R., *et al.*, 2020. Crossing borders and expanding modal shift measures: Effects on mode choice and emissions from freight transport in the Nordics. *Sustainability*, 12 (3), 894.
- Pulugurta, H., Shao, Q., and Chou, Y., 2009. Pavement condition prediction using Markov process. *Journal of Statistics and Management Systems*, 12 (5), 853–871.
- Ranadive, M. and Tapase, A., 2016. Pavement performance evaluation for different combinations of temperature conditions and bituminous mixes. *Innovative Infrastructure Solutions*, 1 (1), 1–5.
- Rue, H., Martino, S., and Chopin, N., 2009a. Approximate Bayesian inference for latent Gaussian models by using integrated nested Laplace approximations. *Journal of the royal statistical society: Series b (statistical methodology)*, 71 (2), 319–392.
- Rue, H., *et al.*, 2017. Bayesian computing with INLA: a review. *Annual Review of Statistics and Its Application*, 4, 395–421.
- Rue, H., Martino, S., and Chopin, N., 2009b. Approximate Bayesian Inference for Latent Gaussian Models by Using Integrated Nested Laplace approximations. *Journal of the Royal Statistical Society Series B*, 71, 319–392.
- Saba, R.G., *et al.*, 2006. Performance prediction models for flexible pavements: A state-of-the-art report.
- Simpson, D., *et al.*, 2017. Penalising model component complexity: A principled, practical approach to constructing priors. *Statistical science*, 32 (1), 1–28.
- Snilsberg, B., 2008. Pavement wear and airborne dust pollution in Norway.

- Spiegelhalter, D.J., *et al.*, 2002. Bayesian measures of model complexity and fit. *Journal of the royal statistical society: Series b (statistical methodology)*, 64 (4), 583–639.
- Standfield, L., Comans, T., and Scuffham, P., 2014. Markov modeling and discrete event simulation in health care: a systematic comparison. *International journal of technology assessment in health care*, 30 (2), 165–172.
- Stephansen, S., 2022. “Norwegian Public Roads Administration”, [<https://www.regjeringen.no/en/dep/sd/organisation/subordinate-agencies-and-enterprises/norwegian-public-roads-administration/id443412/>]. [Online; accessed 19-January-2023].
- Sygna, L. and O’Brien, K., 2001. Virkninger av klimaendringer i Norge. *CICERO Report*. Available from: <http://hdl.handle.net/11250/192050>.
- Taddesse, E., 2013. Intelligent pavement rutting prediction models: the case of Norwegian main road network. In: *Proceedings of the international conferences on the bearing capacity of roads, railways and airfields*. 1051–1060.
- Thodesen, C.C., *et al.*, 2012. Review of asphalt pavement evaluation methods and current applications in Norway. *The Baltic Journal of Road and Bridge Engineering*, 7 (4), 246–252.
- Vedvik, E., 2021. *Spatial non-stationary models for pavement deterioration and traffic accidents*. Thesis (Masters). NTNU.
- vegvesen Vegdirektoratet, S., 2009. General specifications 2: standard specification texts for bridges and quays: principal specification 8:[handbook 026e].
- Vermunt, J.K., Langeheine, R., and Bockenholt, U., 1999. Discrete-time discrete-state latent Markov models with time-constant and time-varying covariates. *Journal of Educational and Behavioral Statistics*, 24 (2), 179–207.
- Watanabe, S. and Opper, M., 2010. Asymptotic equivalence of Bayes cross validation and widely applicable information criterion in singular learning theory. *Journal of machine learning research*, 11 (12).
- Yamany, M.S. and Abraham, D.M., 2020. Prediction of pavement performance using non-homogeneous Markov models: Incorporating the impact of preventive maintenance. In: *Transportation Research Board 99th Annual Meeting, Washington DC*.
- Yan, J., Zhang, H., and Hui, B., 2020. Analysis of the lateral slope’s impact on the calculation of water-filled rut depth. *Plos one*, 15 (12), e0243952.
- Yao, L., *et al.*, 2023. Effects of traffic load amplitude sequence on the cracking performance of asphalt pavement with a semi-rigid base. *International Journal of Pavement Engineering*, 24 (1), 2152027.
- Yu, M., *et al.*, 2023. A prediction model of the friction coefficient of asphalt pavement considering traffic volume and road surface characteristics. *International Journal of Pavement Engineering*, 24 (1), 2160451.
- Zhang, J., *et al.*, 2017. Characterizing the three-stage rutting behavior of asphalt pavement with semi-rigid base by using UMAT in ABAQUS. *Construction and Building Materials*, 140, 496–507.
- Zhang, Q., Yang, S., and Chen, G., 2023. Regional variations of climate change impacts on asphalt pavement rutting distress. *Transportation Research Part D: Transport and Environment*, 103968.
- Zhang, X., *et al.*, 2022. The classification and reutilisation of recycled asphalt pavement binder: Norwegian case study. *Case Studies in Construction Materials*, 17, e01491.
- Zhao, Z., *et al.*, 2020. Factors affecting the rutting resistance of asphalt pavement based on the field cores using multi-sequenced repeated loading test. *Construction and Building Materials*, 253, 118902.

7. Appendices

Appendix A. Inference from model parameters

Table A1 compares estimates from the proposed spatial and non-spatial models. The results show that the spatial models account for uncertainty in factors that vary in space, e.g., weather and other explanatory variables such as bearing capacity and roadside ditches not included in the model. Including more explanatory variables reduces the ‘noise’ term ($\hat{\sigma}_\varepsilon$) and random yearly effect ($\hat{\sigma}_\gamma$).

Table A1.: Estimated model parameters with 95% credible intervals

SPATIAL MODELS						
	Model 1		Model 2		Model 3	
	Mean/Median	95% CI	Mean/Median	95% CI	Mean/Median	95% CI
$\hat{\beta}_{Ac}$	7.13	[6.62, 7.65]	7.19	[6.66, 7.72]	6.98	[6.44, 7.53]
$\hat{\beta}_{Agc}$	7.34	[6.92, 7.76]	7.38	[6.95, 7.81]	7.15	[6.72, 7.59]
$\hat{\beta}_{Sma}$	3.63	[3.37, 3.90]	3.57	[3.30, 3.85]	3.36	[3.08, 3.64]
$\hat{\beta}_{d-1}$	0.74	[0.66, 0.82]	0.77	[0.69, 0.85]	-	-
$\hat{\beta}_w$	-0.10	[-0.14, -0.07]	-	-	-	-
$\hat{\sigma}_{\omega(s)}$	0.47	[0.44, 0.51]	0.48	[0.45, 0.53]	0.52	[0.48, 0.57]
$\hat{\sigma}_\gamma$	0.72	[0.62, 0.88]	0.81	[0.64, 1.09]	0.72	[0.58, 0.94]
$\hat{\sigma}_\varepsilon$	1.38	[1.38, 1.39]	1.38	[1.37, 1.39]	1.39	[1.38, 1.40]

NON-SPATIAL MODELS						
	Model 4		Model 5		Model 6	
	Mean/Median	95% CI	Mean/Median	95% CI	Mean/Median	95% CI
$\hat{\beta}_{Ac}$	3.25	[2.81, 3.68]	3.25	[2.81, 3.69]	2.72	[2.28, 3.16]
$\hat{\beta}_{Agc}$	3.21	[2.75, 3.67]	3.20	[2.74, 3.67]	2.71	[2.24, 3.18]
$\hat{\beta}_{Sma}$	2.00	[1.81, 2.19]	2.02	[1.83, 2.21]	1.55	[1.36, 1.73]
$\hat{\beta}_{d-1}$	1.08	[0.98, 1.18]	1.08	[0.98, 1.18]	-	-
$\hat{\beta}_w$	0.05	[-0.02, 0.11]	-	-	-	-
$\hat{\sigma}_\gamma$	1.38	[0.96, 2.16]	1.45	[0.98, 2.21]	1.43	[0.99, 2.25]
$\hat{\sigma}_\varepsilon$	1.54	[1.53, 1.56]	1.54	[1.53, 1.56]	1.56	[1.54, 1.57]

A.1. Model Comparison

Model comparison criteria (Table A2) select the models with more explanatory variables most often as the best model, with the highest goodness-of-fit (lowest DIC and WAIC). As shown in the results above (e.g., Table A1), the more complex spatial models (Model 1) and non-spatial models (Model 4 or 5) capture the random and spatial variability of pavement rutting and explains more of the unstructured error terms with the addition of explanatory variable lane width.

Table A2.: Model comparison

Model	Estimates from spatial models			Model	Estimates from non-spatial models		
	DIC	WAIC	(-) loglikelihood		DIC	WAIC	(-) loglikelihood
1	193678.05	287136.55	-101455.25	4	104290.62	100995.92	-52229.45
2	194145.55	301922.59	-101459.74	5	104292.58	101057.74	-52223.40
3	193938.88	285335.82	-101625.45	6	104763.18	101615.56	-52453.58

A.2. Marginal Posterior Distributions of Explanatory Variables

Figure A.1 gives the marginal posterior distributions of asphalt type, rut depth from the previous year and lane width. Narrow bands of the distributions indicate that the uncertainty is smaller. Graph (a) shows a clear shift in asphalt type’s contribution to rutting from the spatial and non-spatial models. This is because asphalt type is spatially varying. Stone mastic asphalt (Sma) gave lower rutting values because it has a stronger binder.

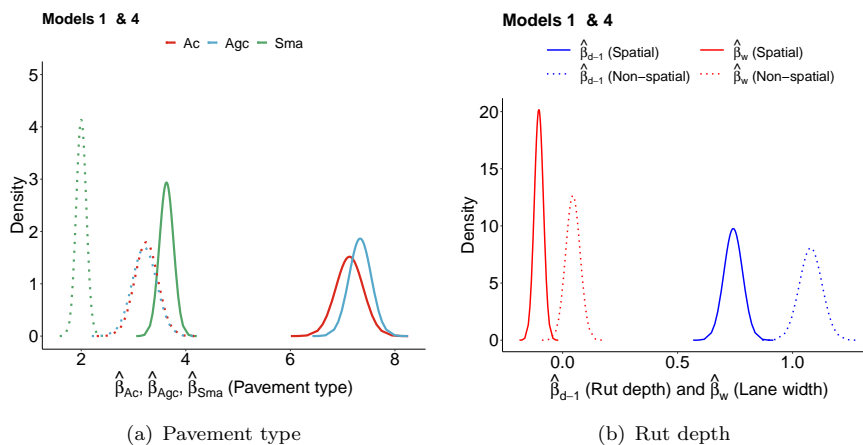


Figure A.1.: Marginal posterior distributions of pavement type (solid lines are the spatial models, and the dotted lines are the non-spatial models), rut depth from the previous year and lane width.

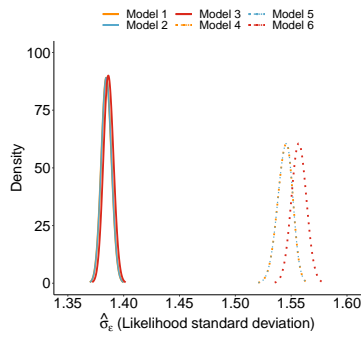
A.3. Marginal Posterior Distributions of Random Effects

Figure A.2 gives the marginal posterior distributions of the standard deviation of the Gaussian observations ($\hat{\sigma}_\varepsilon$), the standard deviation of the random yearly effect ($\hat{\sigma}_\gamma$), the range of the common spatial field $\hat{\rho}$, and the standard deviation of the common spatial field $\hat{\sigma}_{\omega(s)}$. The solid lines represent the spatial models and the dotted lines represent the non-spatial models. Narrower densities suggest smaller estimated uncertainty. We find that some of the uncertainty of the Gaussian observations ($\hat{\sigma}_\varepsilon$) and random yearly effect ($\hat{\sigma}_\gamma$) go into the spatial effect $\{\hat{\sigma}_{\omega(s)}\}$, and this can be interpreted as some of the unobserved variability (e.g., weather, temperature) being explained by the spatial component; see Table 3 and Figure A.2 (a) and (b). This is confirmed by the smaller estimates of the ‘noise’ term ($\hat{\sigma}_\varepsilon$) compared with the non-spatial model

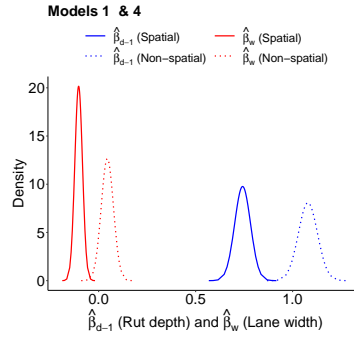
(Table A1).

We examine the effects of the range of the common spatial field ($\hat{\rho}$), and the standard deviation of the common spatial field $\{\hat{\sigma}_{\omega(s)}\}$. As more explanatory variables are added to model (e.g., rut depth), the variability of the common spatial field $\{\hat{\sigma}_{\omega(s)}\}$ decreases; see Figure A.2, graph (d).

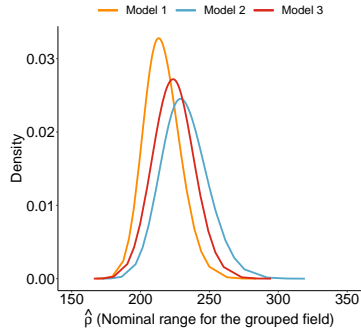
In Model 2, rut depth from the previous year is included, and this effect is large with the credible interval not covering zero. This indicates that deeper rut depths from the previous year would result in increased rutting; Figure A.1, graph (b). In addition, the spatial range for the common spatial field is, generally, larger for Model 2 compared with Model 3 (the simpler model), where rut depth is included (see Table ?? in Supplementary Material ??) for estimated $\hat{\rho}_t$ for each year). This is so, presumably, because of influenced factors such as varying weather patterns. But including lane width reduces the effect of rut depth on expected rutting.



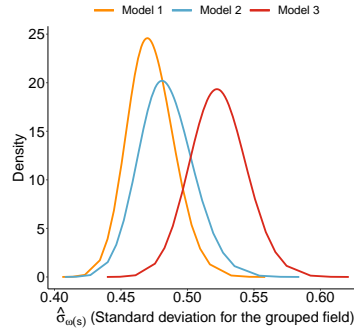
(a) Marginal posterior distributions of the standard deviation of the Gaussian observations $\hat{\sigma}_\epsilon$.



(b) Marginal posterior distributions of the standard deviation of the random yearly effect $\hat{\sigma}_\gamma$.



(c) Marginal posterior distributions of the nominal range of the common spatial field $\hat{\rho}$.



(d) Marginal posterior distributions of the standard deviation of the common spatial field $\hat{\sigma}_{\omega(s)}$.

Figure A.2.: Estimates of marginal posterior distributions of the spatial models (solid lines) and non-spatial models (dotted lines).

ARTICLE TEMPLATE

Supplementary Material: A Spatial-statistical model to analyse historical rutting data.**ARTICLE HISTORY**

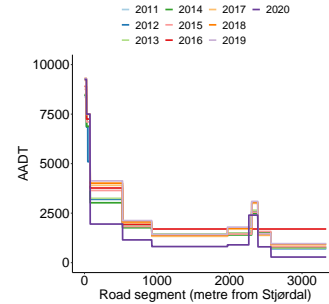
Compiled January 9, 2024

Supplementary Material S1. Data summary

Figure S1.1 gives a summary of the available data used in the analysis. There are a large number of missing values in year 2014. This suggests that repavement took place in this year. The AADT is given in graph (b). The years 2020-2020 gave, in general, the lowest AADT values. This is a result of the COVID-19 pandemic.

Year	Missing rut	Rut	Width	Slope	Min. rutting	Max. rutting
2010	167	3188	3338	816	0	0
2011	1	3354	3338	816	-11.1	40.9
2012	7	3348	3338	816	-8.9	202.2
2013	0	3355	3338	816	-10.7	36.7
2014	1089	2257	3338	816	-9.3	19.6
2015	17	3338	3338	816	-8.9	30.5
2016	0	3355	3338	816	-9.6	19.7
2017	0	3355	3338	816	-5.4	17.2
2018	0	3355	3338	816	-4.5	20.4
2019	0	3355	3338	816	-6.0	15.4
2020	0	3355	3338	816	-5.9	10.1

(a) Summary of rut data



(b) AADT data

Figure S1.1.: Available rut depth, road width, slope height measurements, and minimum and maximum rutting are shown. Year 2014 has (\sim) 32% NaNs for rut depth, suggesting that re-pavement has taken place at these locations. This means that the correlation between rut depth values will be fast deteriorating with distance, suggesting a small spatial range process.

Supplementary Material S2. Matérn covariance structure

The annually varying spatial process $\xi_t(\mathbf{s})$ is a Gaussian random process $\{\xi_t(\mathbf{s}) : \mathbf{s} \in \mathcal{D} \subseteq \mathbb{R}^d\}$ such that for any $n \geq 1$ and for each set of spatial locations (s_1, \dots, s_n) satisfies

$$\xi_t(\mathbf{s}) = \{\xi_t(s_1), \dots, \xi_t(s_n)\} = (\xi_{t,1}, \dots, \xi_{t,n}) \sim \text{Normal}(\boldsymbol{\mu}, \boldsymbol{\Sigma}). \quad (\text{S21})$$

Here $\boldsymbol{\mu} = \{\mu(s_1), \dots, \mu(s_n)\}$ is the mean vector and $\Sigma_{ij} = \text{Cov}\{\xi_t(s_i), \xi_t(s_j)\} = C\{\xi_t(s_i), \xi_t(s_j)\}$ are the elements of the covariance matrix defined by the Matérn stationary

isotropic covariance function

$$C \{ \xi_t(s_i), \xi_t(s_j) \} = \frac{\sigma_{\xi_t}^2}{2^{\nu-1} \Gamma(\nu)} (\kappa \|s_i - s_j\|_2)^\nu K_\nu(\kappa \|s_i - s_j\|_2), \quad (\text{S22})$$

for $s_i, s_j \in \mathcal{D}$, where $\|\cdot\|_2$ denotes the Euclidean distance. The scaling parameter is $\kappa > 0$; K_ν is the modified Bessel function of second order kind and order $\nu = \alpha - d/2 > 0$ such that $\alpha = \nu + d/2$, which controls the smoothness of the realisations; and $\sigma_{\xi_t}^2$ is the marginal variance defined as:

$$\sigma_{\xi_t}^2 = \frac{\Gamma(\nu)}{(4\pi)^{d/2} \Gamma(\alpha) \kappa^{2\nu} \tau^2}.$$

Similarly, the common spatial process $\omega(s)$ is a Gaussian random process $\{\omega(s) : s \in \mathcal{D} \subseteq \mathbb{R}^d\}$ defined as

$$\omega(s) = \{\omega(s_1), \dots, \omega(s_n)\} = (\omega_1, \dots, \omega_n) \sim \text{Normal}(\boldsymbol{\mu}^\omega, \Sigma^\omega), \quad (\text{S23})$$

where $\boldsymbol{\mu}^\omega = \{\mu^\omega(s_1), \dots, \mu^\omega(s_n)\}$ is the mean vector and $\Sigma_{ij}^\omega = \text{Cov}\{\omega(s_i), \omega(s_j)\} = C^\omega\{\omega(s_i), \omega(s_j)\}$ are the elements of Matérn stationary isotropic covariance function defined in Equation (S22), but with marginal variance defined as $\sigma_{\omega(s)}^2$; the scaling parameter given as $\kappa_\omega > 0$; and with K_{ν_ω} defined as the modified Bessel function of second order kind and order $\nu_\omega = \alpha_\omega - d/2 > 0$.

Following Lindgren *et al.* (2011), $\omega(s)$ and $\xi_t(s)$ are modelled with a stationary SPDE (stochastic partial differential equation) approach (Ingebrigtsen *et al.* 2014, Blangiardo and Cameletti 2015, Ingebrigtsen *et al.* 2015, Krainski *et al.* 2018), with form

$$\mathcal{W}(s) = (\kappa^2 - \Delta)^{\alpha/2} (\tau \xi_t(s)). \quad (\text{S24})$$

or

$$\mathcal{W}_\omega(s) = (\kappa_\omega^2 - \Delta)^{\alpha_\omega/2} (\tau_\omega \omega(s)). \quad (\text{S25})$$

respectively, where Δ is the Laplacian; τ (or τ_ω) controls the variance; and $\mathcal{W}(s)$ or $\{\mathcal{W}_\omega(s)\}$ is the Gaussian spatial white noise. The solutions to the SPDEs are the stationary Gaussian random fields $\xi_t(s)$ and $\omega(s)$. With this SPDE approach, the Matérn field is represented by a linear combination of basis functions defined in a triangulation of a given spatial domain \mathcal{D} (Juan Verdoy 2021). In this paper, the spatial domain along Highway road E14 is assumed to be one-dimensional ($d = 1$), with a triangulation having vertices every 20th metre or one road segment.

Instead of using the scaling parameter κ_ω (or κ), it is common to use the spatial range ρ for the common spatial field (or ρ_t for the annually varying spatial field) defined empirically as

$\rho = 2\sqrt{2\nu_\omega/\kappa_\omega}$. Here, we assume the default value $\alpha_\omega = 2$ in R-INLA, such that $\nu_\omega = 3/2$, and the commonly used spatial range ρ and marginal variance of the spatial field $\sigma_{\omega(s)}^2$:

$$\rho = \frac{2\sqrt{3}}{\kappa_\omega} \quad \text{and} \quad \sigma_{\omega(s)}^2 = \frac{1}{4\kappa_\omega^3\tau_\omega^2}. \quad (\text{S26})$$

Supplementary Material S3. Additional Results

Here, we give some additional results of the inference and random effects obtained from the spatial models.

S3.1. Inference from the explanatory variables

S3.1.1. Pavement type

The fixed effect of pavement type on expected annual rutting from all models is given in Figure S3.1. The effect of asphalt concrete (Ac) and asphalt gravel concrete (Agc) on expected annual rutting is very clear when the spatial effects are considered (solid lines). Also, the uncertainty from using either of the pavement types is also clearly identified, with stone mastic asphalt type (Sma) having the smallest variability. When the spatial effects of pavement type is not considered, the effects on rutting are not easily distinguishable (dotted lines).

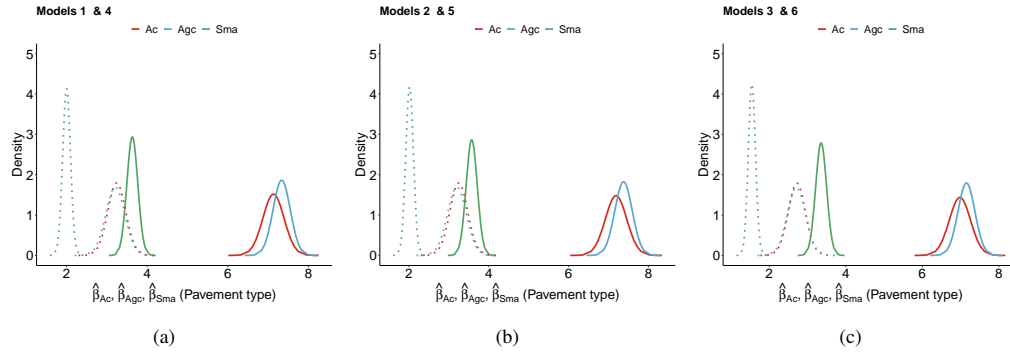


Figure S3.1.: Marginal posterior distributions of pavement type. Solid lines are the spatial models and the dotted lines are the non-spatial models.

S3.1.2. Rut depth and Lane width

Estimates of rut depth from the previous year are smaller, including the uncertainty, from the spatial models compared with non-spatial models (Figure S3.2, graph (a)). Some of this uncertainty of the rut depth from the spatial models is captured in the common spatial field and the random year. Estimated lane width is negative, suggesting that narrower roads allow for more rutting rates; Figure S3.2, graph (b).

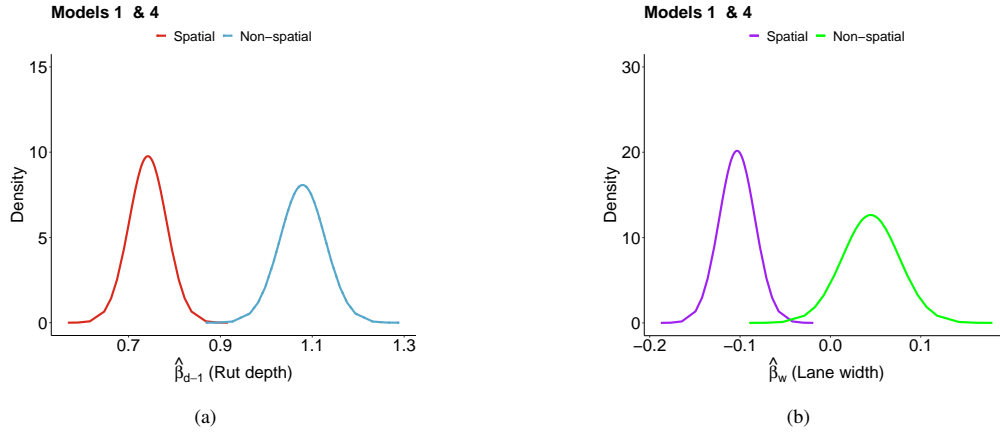


Figure S3.2.: Marginal posterior distributions for rut depth from the previous year and lane width from spatial and non-spatial models.

S3.2. Inference from random effects

The estimated random yearly effect $\hat{\gamma}$ from the non-spatial models is much larger than that of the spatial models.

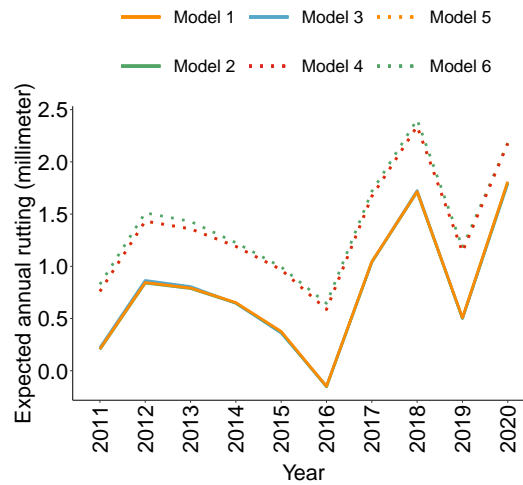


Figure S3.3.: Expected annual rutting, $\hat{\gamma}_t$.

The estimated nominal range $\hat{\rho}_t$ (Table S3.1) is quite variable, especially for the later years 2017-2020. We see that $\hat{\rho}_{2014}$ is also quite large. There were large-scale maintenance activities in 2014 (see Section S1) and, therefore, the correlation between rut depth values will be fast deteriorating with distance, indicating a small spatial range process. The marginal standard deviation of the spatial field for each year $\hat{\sigma}_{\xi,t}$ (Table S3.2) is less than 2.5 metres, the prior knowledge of the value of GMF at an arbitrary location. This means that with prior knowledge, reasonable and credible intervals are achieved.

Table S3.1.: Estimated nominal range for each year $\hat{\rho}_t$, with 95% credible intervals.

Year	Model 3		Model 2		Model 1	
	$\hat{\rho}_t$	95% CI	$\hat{\rho}_t$	95% CI	$\hat{\rho}_t$	95% CI
2011	101.54	[87.95, 117.85]	96.76	[83.25, 112.00]	97.83	[85.51, 112.00]
2012	1853.01	[1302.36, 2554.821]	2050.08	[1489.63, 2800.00]	2111.54	[1520.10, 2930.00]
2013	72.18	[57.32, 90.41]	64.83	[50.82, 82.90]	65.99	[54.27, 81.91]
2014	2147.65	[1394.70, 3270.82]	2497.48	[1427.90, 4290.00]	2161.97	[1501.98, 3110.00]
2015	138.87	[107.71, 176.65]	137.83	[105.34, 177.00]	137.57	[109.91, 1690.00]
2016	578.49	[369.97, 848.90]	627.96	[401.72, 907.00]	546.29	[368.79, 768.00]
2017	4188.29	[2836.92, 6027.91]	5604.44	[3242.25, 9570.00]	4570.15	[3167.12, 6510.00]
2018	6203.25	[4189.73, 9012.55]	8127.93	[5200.82, 12000.00]	7911.90	[5420.41, 1130.00]
2019	4298.92	[4992.61, 9885.86]	5149.90	[3386.66, 7760.00]	5721.98	[3613.91, 8970.00]
2020	7138.28	[4992.61, 9885.86]	8419.42	[5754.69, 12200.00]	9004.09	[6473.55, 12400.00]

Table S3.2.: Estimated standard deviation of the spatial field for each year $\hat{\sigma}_{\xi_t}$, with 95% credible intervals.

Year	Model 3		Model 2		Model 1	
	$\hat{\sigma}_{\xi_t}$	95% CI	$\hat{\sigma}_{\xi_t}$	95% CI	$\hat{\sigma}_{\xi_t}$	95% CI
2011	1.62	[1.53, 1.72]	1.60	[1.50, 1.69]	1.61	[1.51, 1.70]
2012	1.34	[1.08, 1.63]	1.30	[1.04, 1.62]	1.28	[1.04, 1.55]
2013	1.71	[1.60, 1.82]	1.73	[1.62, 1.85]	1.73	[1.63, 1.83]
2014	1.01	[0.76, 1.32]	1.01	[0.76, 1.30]	1.01	[0.80, 1.25]
2015	1.07	[0.98, 1.14]	1.07	[0.97, 1.18]	1.07	[0.99, 1.16]
2016	0.53	[0.45, 0.63]	0.51	[0.41, 0.68]	0.51	[0.44, 0.59]
2017	1.01	[0.79, 1.27]	0.96	[0.73, 1.26]	0.95	[0.76, 1.18]
2018	1.39	[1.06, 1.80]	1.39	[0.99, 1.87]	1.36	[1.01, 1.83]
2019	0.55	[0.41, 0.73]	0.49	[0.37, 0.64]	0.51	[0.39, 0.67]
2020	1.50	[0.71, 1.14]	1.52	[1.08, 2.10]	1.51	[1.14, 1.96]

References

- Blangiardo, M. and Cameletti, M., 2015. *Spatial and spatio-temporal Bayesian models with R-INLA*. John Wiley & Sons.
- Ingebrigtsen, R., Lindgren, F., and Steinsland, I., 2014. Spatial models with explanatory variables in the dependence structure. *Spatial Statistics*, 8, 20–38.
- Ingebrigtsen, R., *et al.*, 2015. Estimation of a non-stationary model for annual precipitation in southern Norway using replicates of the spatial field. *Spatial Statistics*, 14, 338–364.
- Juan Verdoy, P., 2021. Enhancing the SPDE modeling of spatial point processes with INLA, applied to wildfires. Choosing the best mesh for each database. *Communications in Statistics-Simulation and Computation*, 50 (10), 2990–3030.
- Krainski, E., *et al.*, 2018. *Advanced spatial modeling with stochastic partial differential equations using R and INLA*. Chapman and Hall/CRC.
- Lindgren, F., Rue, H., and Lindström, J., 2011. An explicit link between Gaussian fields and Gaussian Markov random fields: the stochastic partial differential equation approach. *Journal of the Royal Statistical Society: Series B (Statistical Methodology)*, 73 (4), 423–498.